5106 *Inorg. Chem.* **2009**, *48*, 5106–5116
DOI: 10.1021/ic802440h

Inorganic Chemistry
Article

# Ligand Dependence of Binding to Three-Coordinate Fe(II) Complexes

**Karen P. Chiang,[†] Pamela M. Barrett,[†] Feizhi Ding,[‡] Jeremy M. Smith,[‡] Savariraj Kingsley,[†] William W. Brennessel,[†] Meghan M. Clark,[†] Rene J. Lachicotte,[†] and Patrick L. Holland*[,†]**

[†]*Department of Chemistry, University of Rochester, Rochester, New York 14627, and* [‡]*Department of Chemistry and Biochemistry, New Mexico State University, Las Cruces, New Mexico 88003*

Received December 24, 2008

A series of three- and four-coordinate iron(II) complexes with nitrogen, chlorine, oxygen, and sulfur ligands is presented. The electronic variation is explored by measuring the association constant of the neutral ligands and the reduction potential of the iron(II) complexes. Varying the neutral ligand gives large changes in $K_{eq}$, which decrease in the order $CN^tBu$ > pyridine >2-picoline > DMF > MeCN > THF > $PPh_3$. These differences can be attributed to a mixture of steric effects and electronic effects (both $\sigma$-donation and $\pi$-backbonding). The binding constants and the reduction potentials are surprisingly insensitive to changes in an anionic spectator ligand. This suggests that three-coordinate iron(II) complexes may have similar binding trends as proposed three-coordinate iron(II) intermediates in the FeMoco of nitrogenase, even though the anionic spectator ligands in the synthetic complexes differ from the sulfides in the FeMoco.

## Introduction

Nitrogenases are fascinating iron metalloenzymes that have the ability to convert dinitrogen to ammonia at ambient temperature and pressure.[1,2] They also reduce a variety of organic substrates such as alkynes, nitriles, cyanide, isocyanide, $CO_2$, azide, nitrous oxide, and cyclopropene.[3] So far, scientists have not unambiguously determined the binding location of any substrate in a nitrogenase enzyme.

The current "best guesses" for substrate binding sites are based on a 1.16 Å resolution structure of the resting state of the iron−molybdenum nitrogenase from *A. vinelandii*.[4] The active site of the iron−molybdenum enzyme is a cluster called the FeMo cofactor (FeMoco), identified as $MoFe_7S_9X$(homocitrate), where X represents $C^{4-}$, $N^{3-}$, or $O^{2-}$ (Figure 1). Other nitrogenases lack molybdenum but have a similarly shaped cluster, based on Extended X-ray Absorption Fine Structure (EXAFS) evidence.[5]

One reasonable hypothesis for the location of substrate binding on the FeMoco is the iron atoms in the "belt" of the enzyme, and this idea has been supported by the substrate dependence of nitrogenase mutants.[7,8] Even though the belt iron atoms are four-coordinate in the crystallographically characterized resting state, they could become three-coordinate and coordinatively unsaturated in the reduced form that binds substrates.[9] This idea has motivated the study of isolable three-coordinate iron(II) complexes that mimic the "activated" three-coordinate sites on the FeMoco.[6,10−12]

Though it might be most desirable to study iron complexes with three sulfur donors, the available S-coordinated three-coordinate Fe complexes have a highly congested iron environment, and are prone to ligand dissociation.[13,14] We have focused instead on three-coordinate complexes in which two of the donors come from a bulky $\beta$-diketiminate ligand ($L^{tBu,iPr2}$, Scheme 1), because these complexes are easy to prepare, highly crystalline, and suitable for detailed spectroscopic and mechanistic analysis.[15] One potential point

*To whom correspondence should be addressed. E-mail: holland@chem.rochester.edu.

(1) Holland, P. L. In *Comprehensive Coordination Chemistry II*; McCleverty, J., Meyer, T. J., Eds.; Elsevier: Oxford, 2004; Vol. *8*, p 569−599.
(2) Barney, B. M.; Lee, H.-I.; Dos Santos, P. C.; Hoffman, B. M.; Dean, D. R.; Seefeldt, L. C. *Dalton Trans*. **2006**, 2277–2284.
(3) Burgess, B. K.; Lowe, D. J. *Chem. Rev*. **1996**, *96*, 2983–3011.
(4) Einsle, O.; Tezcan, F. A.; Andrade, S. L. A.; Schmid, B.; Yoshida, M.; Howard, J. B.; Rees, D. C. *Science* **2002**, *297*, 1696–1700.
(5) Krahn, E.; Weiss, B. J. R.; Kröckel, M.; Groppe, J.; Henkel, G.; Cramer, S. P.; Trautwein, A. X.; Schneider, K.; Müller, A. *J. Biol. Inorg. Chem*. **2002**, *7*, 37–45.
(6) Holland, P. L. *Can. J. Chem*. **2005**, *83*, 296–301.
(7) Seefeldt, L. C.; Dance, I. G.; Dean, D. R. *Biochemistry* **2004**, *43*, 1401–1409.
(8) Dos Santos, P. C.; Igarashi, R. Y.; Lee, H.-I.; Hoffman, B. M.; Seefeldt, L. C.; Dean, D. R. *Acc. Chem. Res*. **2005**, *38*, 208–214.
(9) Schimpl, J.; Petrilli, H. M.; Blöchl, P. E. *J. Am. Chem. Soc*. **2003**, *125*, 15772–15778.
(10) Smith, J. M.; Sadique, A. R.; Cundari, T. R.; Rodgers, K. R.; Lukat-Rodgers, G.; Lachicotte, R. J.; Flaschenriem, C. J.; Vela, J.; Holland, P. L. *J. Am. Chem. Soc*. **2006**, *128*, 756–769.
(11) Lees, N. S.; McNaughton, R. L.; Gregory, W. V.; Holland, P. L.; Hoffman, B. M. *J. Am. Chem. Soc*. **2008**, *130*, 546–555.
(12) Yu, Y.; Sadique, A. R.; Smith, J. M.; Dugan, T. R.; Cowley, R. E.; Brennessel, W. W.; Flaschenriem, C. J.; Bill, E.; Cundari, T. R.; Holland, P. L. *J. Am. Chem. Soc*. **2008**, *130*, 6624–6638.
(13) MacDonnell, F. M.; Ruhlandt-Senge, K.; Ellison, J. J.; Holm, R. H.; Power, P. P. *Inorg. Chem*. **1995**, *34*, 1815–1822.
(14) Lee, S. C.; Holm, R. H. *Proc. Natl. Acad. Sci. U.S.A*. **2003**, *100*, 3595–3600.
(15) Holland, P. L. *Acc. Chem. Res*. **2008**, *41*, 905–914.


Published on Web 05/12/2009

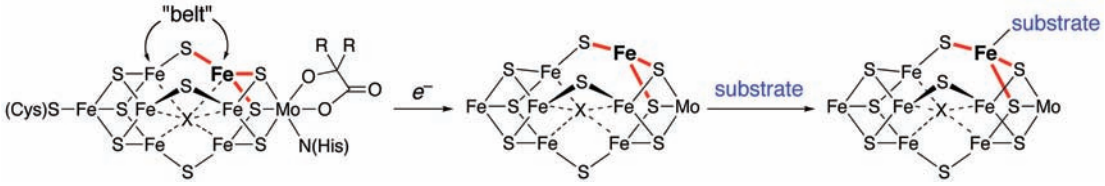


**Figure 1.** FeMoco of iron−molybdenum nitrogenase in the resting state.[4] X is a light atom (C, N, or O) that lies 2.0 Å from the six "belt" iron atoms. The iron atoms along the "belt" are coordinated to three bridging sulfides. We hypothesize that reduction of the cofactor transiently gives a three-coordinate iron site that can bind substrate.[6]

**Scheme 1**

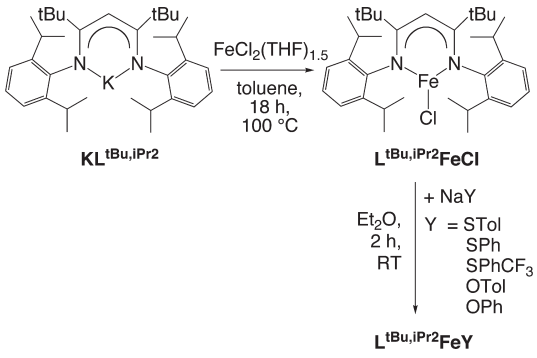


of concern is that the identity of the donor atoms to iron is different in the $\beta$-diketiminate complexes (N donors) than in the FeMoco (S donors). It is reasonable to suspect that this difference in spectator ligands might influence the binding constants and redox potentials, invalidating the $\beta$-diketiminate complexes as informative nitrogenase mimics. Therefore, it is of interest to learn the influence of spectator ligands on binding to three-coordinate iron complexes. In this paper, we vary one of the three donors in three-coordinate iron complexes, and measure the binding constant ($K_{assoc}$) of a number of neutral ligands to gain systematic knowledge about the trends in these complexes.

There are more general implications as well. First, the binding preferences of trigonal-planar iron complexes are not well understood.[16,17] Also, the influence of spectator ligands on binding constants of neutral ligands is of general interest in coordination chemistry and catalysis and has rarely been studied quantitatively for a range of different types of ligands. Binding of neutral ligands to porphyrin-iron complexes has been studied in some detail, but can be complicated by spin state changes upon binding.[18−20] In contrast, the iron(II) complexes studied here are always high-spin as three- or four-coordinate complexes.

## Results

**Synthesis of Three-Coordinate Fe$^{II}$ Complexes.** We have shown that L$^{tBu,iPr2}$FeCl[21] is a versatile starting material for the synthesis of a variety of three-coordinate iron(II) compounds.[15] In previous studies, L$^{tBu,iPr2}$FeCl was synthesized from reaction of $FeCl_2(THF)_{1.5}$ and the lithium salt of the diketiminate ligand, producing LiCl as a byproduct. Unfortunately, the solubilities of LiCl and L$^{tBu,iPr2}$FeCl are not different enough to enable easy separation of the compounds without Soxhlet extraction, which is inconvenient on a large scale. Here, this difficulty is avoided by using the potassium salt of the bulky $\beta$-diketiminate ligand (KL$^{tBu,iPr2}$). This potassium salt was synthesized by treating HL$^{tBu,iPr2}$ with benzylpotassium[22] in diethyl ether.[23] Reaction of KL$^{tBu,iPr2}$ with $FeCl_2(THF)_{1.5}$ in toluene reproducibly gave a clean product from which KCl could be removed by filtration. L$^{tBu,iPr2}$FeCl was isolated as red crystals in very high yield (97%).

Double-metathesis reactions of L$^{tBu,iPr2}$FeCl led to three-coordinate iron-thiolate (L$^{tBu,iPr2}$FeSPh, L$^{tBu,iPr2}$-FeSPhCF$^3$, L$^{tBu,iPr2}$FeSTol) and phenoxide (L$^{tBu,iPr2}$-FeOPh, L$^{tBu,iPr2}$FeOTol)[24] complexes. In some of these compounds, para-substituents on the aryl rings were used to enable isolation of single crystals, or to introduce an electronic effect (see below). Reactions of L$^{tBu,iPr2}$FeCl and 1 equiv of the appropriate sodium salt were carried out in diethyl ether at room temperature. The complexes were isolated as red-orange crystals by cooling pentane solutions, in yields of 70−85%. The purity of these compounds was typically ascertained using UV−vis spectroscopy, which showed a characteristic visible band in each complex between 500−600 nm, and using $^1$H NMR spectroscopy.

As with other three-coordinate iron(II) diketiminate complexes,[15] the $^1$H NMR spectra had peaks over a range from roughly +120 to −120 ppm. The signals could be integrated to give tentative assignments. In cases where this left ambiguity, resonances were assigned based on proximity to the paramagnetic iron(II) center (protons closer to the metal center are shifted further from 0 ppm).[15] The number of resonances in the spectra are as expected for averaged $C_{2v}$ symmetry, indicating rapid rotation around the Fe−S, Fe−O, S−C, and O−C bonds on the NMR time scale. The Evans method[25,26] was used to calculate the solution magnetic moments, which were 5.5 ± 0.4 Bohr magnetons for all compounds. This indicates a ground state of $S$ = 2, consistent with the expectations for high-spin Fe(II) with substantial orbital

(16) Cummins, C. C. *Prog. Inorg. Chem.* **1998**, *47*, 685–836.
(17) Alvarez, S. *Coord. Chem. Rev.* **1999**, *193−195*, 13–41.
(18) Sanders, J. K. M.; Bampos, N.; Clyde-Watson, Z.; Darling, S. L.; Hawley, J. C.; Kim, H.-J.; Mak, C. C.; Webb, S. J. *Porphyrin Handbook* **2000**, *3*, 1–48.
(19) Ellis, P. E.; Jones, R. D., Jr.; Basolo, F. *J. Chem. Soc., Chem. Commun.* **1980**, 54–55.
(20) Ellis, P. E.; Linard, J. E.; Szymanski, T.; Jones, R. D.; Budge, J. R.; Basolo, F. *J. Am. Chem. Soc.* **1980**, *102*, 1889–1896.
(21) Smith, J. M.; Lachicotte, R. J.; Holland, P. L. *Chem. Commun.* **2001**, 1542–1543.
(22) Bailey, P. J. C., R. A.; Dick, C. M.; Fabre, S.; Henderson, L. C.; Herber, C.; Liddle, S. T.; Lorono-Gonzalez, D.; Parkin, A.; Parsons, S. *Chem. Eur. J.* **2003**, *9*, 4820–4828.
(23) Adhikari, D.; Tran, B. L.; Zuno-Cruz, F. J.; Sanchez Cabrera, G.; Mindiola, D. J.; Chiang, K. P.; Cowley, R. E.; Dugan, T. R.; Holland, P. L. *Inorg. Synth.*, in press.
(24) Eckert, N. A.; Smith, J. M.; Lachicotte, R. J.; Holland, P. L. *Inorg. Chem.* **2004**, *43*, 3306–3321.
(25) Schubert, E. M. *J. Chem. Educ.* **1992**, *69*, 62.
(26) Evans, D. F. *J. Chem. Soc.* **1959**, 2003–2005.

**Table 1.** Relevant Bond Lengths and Angles[a]

| bond/angle | $L^{tBu,iPr2}Fe(SPh)$ | $L^{tBu,iPr2}Fe(STol)$ | $L^{tBu,iPr2}Fe(SPhCF_3)$ | $L^{tBu,iPr2}Fe(OTol)$ |
|---|---|---|---|---|
| Fe−N (Å) | 1.959(2) | 1.969(1) | 1.960(1) | 1.965(2) |
| | 1.969(2) | 1.971(1) | 1.968(1) | 1.972(2) |
| Fe−E (Å) | 2.2523(6) | 2.2584(5) | 2.2642(5) | 1.833(2) |
| N−Fe−N (deg) | 95.20(6) | 94.49(5) | 94.94(5) | 94.76(8) |
| N−Fe−E (deg) | 144.69(5) | 146.28(4) | 146.97(4) | 140.20(8) |
| | 119.98(5) | 118.56(4) | 117.13(4) | 125.01(9) |
| Fe−E−C (deg) | 110.06(7) | 114.37(5) | 114.70(5) | 138.8(2) |

[a] E represents S or O.

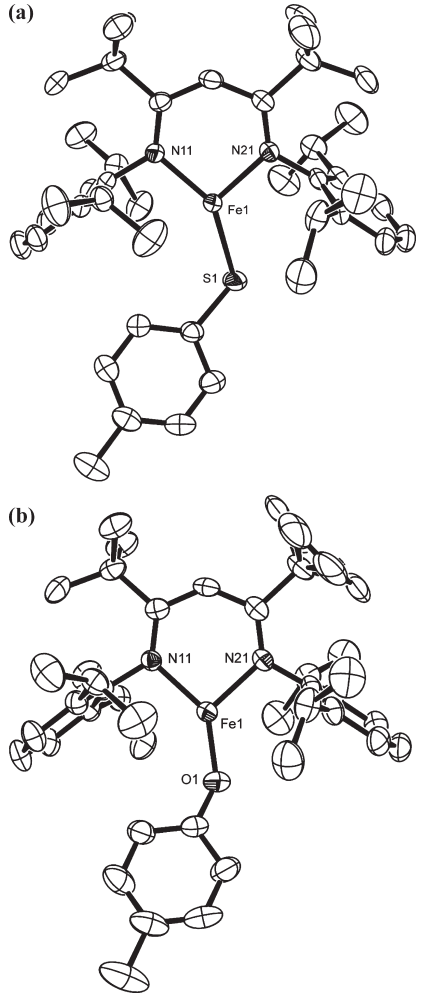


**Figure 2.** ORTEP drawings of the molecular structures of (a) $L^{tBu,iPr2}FeSTol$ and (b) $L^{tBu,iPr2}Fe(OTol)$. Analogous drawings of $L^{tBu,iPr2}Fe(SPh)$ and $L^{tBu,iPr2}Fe(SPhCF_3)$ are given in the Supporting Information. Thermal ellipsoids are shown at 50% probability. Hydrogen atoms have been omitted for clarity.

angular momentum, as studied in detail for $L^{tBu,iPr2}FeCl$ and $L^{tBu,iPr2}FeCH_3$.[27]

The molecular structures of $L^{tBu,iPr2}FeSPh$, $L^{tBu,iPr2}$-$FeSTol$, $L^{tBu,iPr2}FeSPhCF_3$, and $L^{tBu,iPr2}FeOTol$ were determined by X-ray crystallography. Thermal-ellipsoid plots of the crystallographic models are shown in Figure 2, and relevant bond lengths and angles are given in Table 1. The iron centers are planar, and the sum of the three angles is greater than 359°.[21,24,28] Interestingly, the sulfur atoms lie off the $C_2$ axis of the diketiminate-iron group, giving N−Fe−S angles that differ by 25°, 28°, and 30° in the three thiolate complexes. The cause for this "T" shape may be that the sulfur atom prefers a relatively small angle. The Fe−S−C angles in our complexes range from 110° to 115°, which fall close or within a standard deviation of the average Fe−S−C angle, 110(4)°, in the Cambridge Structural Database (CSD). To accommodate a thiolate ligand with this Fe−S−C angle between the bulky aryl rings of the diketiminate, the iron coordination must distort. In the aryloxide complex $L^{tBu,iPr2}FeOTol$, the angle at oxygen is somewhat larger at 138.8(2)°, also within a standard deviation of the average Fe−O−C angle in the CSD, 133(8)°. Because the larger angle at oxygen causes less steric pressure on the iron coordination geometry, the N−Fe−O angles in the aryloxide complex are more similar ($\Delta \sim 15°$) than in the more distorted thiolates ($\Delta \sim 25-30°$).

**Cyclic Voltammetry Studies of Iron(II) Complexes.** The redox chemistry of the three-coordinate complexes was examined using cyclic voltammetry in diethyl ether ($Et_2O$) with 0.1 M $NBu_4BArF$ as electrolyte (BArF = tetrakis[3,5-bis(trifluoromethyl)phenyl]borate). The use of this unusual solvent/electrolyte combination is necessary because more polar solvents like tetrahydrofuran (THF) and acetonitrile (MeCN) coordinate to the iron atom, as shown below.

The complexes show reversible reductions at the low potential of −2.4 to −2.6 V vs ferrocene, which we ascribe to an iron(II)/iron(I) couple (Figure 3). Peak separation ($E_{pa} - E_{pc}$) values for the iron(II)/iron(I) couple are between 100 mV and 200 mV, which is typical for solvents of relatively low polarity.[29] Additionally, an irreversible oxidation ($E_{pa}$) occurs between +0.3 to +0.5 V (for example, see Figure 3a). We have not explored the oxidation products.

The cyclic voltammetry of the complexes was also measured in acetonitrile (MeCN) with 0.1 M $NBu_4PF_6$ electrolyte. As discussed below, MeCN binds to these three-coordinate complexes to give a four-coordinate solvent adduct at high concentrations of MeCN. Therefore, results obtained in MeCN reflect the redox behavior of the four-coordinate complex $L^{tBu,iPr}Fe(Y)(NCMe)$. These four-coordinate complexes showed a quasireversible reduction at low potential and an irreversible oxidation ($E_{pa}$) at 0 to +0.3 V. The only difference between the different complexes is that $L^{tBu,iPr2}FeOPh$ possesses

(27) Andres, H.; Bominaar, E.; Smith, J. M.; Eckert, N. A.; Holland, P. L.; Münck, E. *J. Am. Chem. Soc.* **2002**, *124*, 3012–3025.
(28) Vela, J.; Smith, J. M.; Yu, Y.; Ketterer, N. A.; Flaschenriem, C. J.; Lachicotte, R. J.; Holland, P. L. *J. Am. Chem. Soc.* **2005**, *127*, 7857–7870.
(29) Barriere, F.; LeSuer, R. J.; Geiger, W. E. *Trends Mol. Electrochem.* **2004**, 413–444.

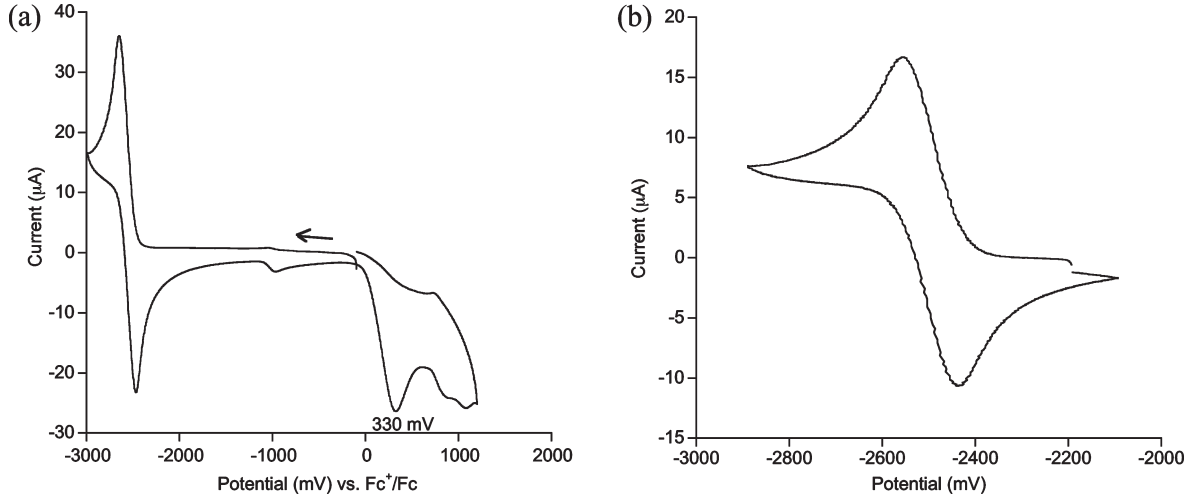


**Figure 3.** Voltammograms of $L^{tBu,iPr2}FeCl$ in $Et_2O$ with 0.1 M $NBu_4BArF$ electrolyte. (a) Full scan at 500 mV/s. (b) The $Fe^{2+/1+}$ wave at 100 mV/s. Other voltammograms are given in the Supporting Information.

**Table 2.** $E_{1/2}$ Values for Reduction of Complexes $L^{tBu,iPr2}FeY$ in $Et_2O$/$NBu_4BArF$ and $L^{tBu,iPr2}FeY(NCMe)$ in $MeCN/NBu_4PF_6$[a]

| Y | $Et_2O$ | MeCN |
|---|---|---|
| Cl | −2.46(1) | −2.32(2) |
| OPh | −2.56(3) | −2.27(6) |
| SPh | −2.41(2) | −2.30(6) |
| $SPhCF_3$ | −2.40(2) | −2.33(1) |

[a] Potentials are given in volts relative to the ferrocenium/ferrocene couple at 0 V.[30,31]

an additional quasireversible response corresponding to an oxidation at $E_{1/2} = -93$ mV.

The $E_{1/2}$ values for the iron(II)/iron(I) couple in both solvents are shown in Table 2. These values are averages from scans with sweep rates between 100−1000 mV/s and are referenced to the ferrocene couple (+0.64 V vs NHE).[30,31] A precipitate formed during the measurement of $L^{tBu,iPr2}$-Fe(OPh)(NCMe), which caused the peak to shift in the negative direction. This change is reflected in the larger error (±60 mV) associated with the $L^{tBu,iPr2}Fe(OPh)$ complex. Although these reduction potentials do not strictly represent thermodynamic potentials, they can be used for comparison of the complexes as described below in the Discussion section.

**Characterization of Four-Coordinate Fe(II) Complexes.** Each of the three-coordinate iron(II) complexes was capable of binding an additional neutral ligand. The amount of added ligand necessary to ensure binding was different depending on the ligand (see below), but was always accompanied by a change from red to an orange color.

The four-coordinate iron(II) complexes have broader $^1H$ NMR spectra than the three-coordinate iron(II) complexes, and fall in a narrower chemical shift range (see Supporting Information). This was observed for every added ligand, suggesting that the broader peaks arise not from ligand exchange but rather from slower electronic relaxation in the four-coordinate complexes. Consistent with this idea, $^1H$ NMR spectra like these have been observed previously for four-coordinate iron(II) diketiminate complexes.[32]

To verify the geometry of the adducts, we determined the solid-state structures of $L^{tBu,iPr2}Fe(SPh)(L)$ (L = *tert*-butyl isocyanide, $CN^tBu$; 1-methylimidazole, MeIm; *N, N*-dimethylformamide, DMF) using X-ray crystallography. Thermal-ellipsoid plots are shown in Figure 4, and important bond lengths and angles are listed in Table 3. The fourth donor binds from the direction normal to the plane of the three-coordinate complexes: the angles between the $N_2S$ plane and the Fe−L bond were 77°, 86°, and 83° in the three structures. This is consistent with the trigonal-pyramidal geometry observed previously in some ligand adducts of $L^{tBu,iPr2}FeCl$.[24,28]

The greater coordination number in the ligand adducts increased the lengths of the bonds to the spectator ligands. The Fe−S bond length on average increased 0.035(2) Å while the Fe−N bonds increased 0.0526(4) Å from the three-coordinate thiolate complex $L^{tBu,iPr2}Fe(SPh)$. The difference between the two N−Fe−S angles within the same complex ranged from 12°−18°, as in the three-coordinate thiolate complexes. The M−S−C angles are typical of those found in the CSD (109 ± 4°).

**Binding Constants of Neutral Donors to $L^{tBu,iPr2}FeCl$, $L^{tBu,iPr2}Fe(SPh)$, $L^{tBu,iPr2}Fe(SPhCF_3)$, and $L^{tBu,iPr2}Fe(OPh)$.** We determined the trends in the binding constants for added neutral ligands, as a function of the added ligand (L) and of the anionic spectator ligand (Y). To carry out the binding studies we monitored the visible absorbance peak of the three-coordinate iron complexes using UV−vis spectrophotometry.

For these experiments, 10 mM stock solutions of the three-coordinate complexes in toluene were sequentially diluted to give samples that were 1.0 mM in $L^{tBu,iPr2}FeY$. The donor ligand, L, was present in amounts varying from 0.25 mM to 1.0 M. A color change from red to orange is observed depending on the particular ligand and amount added. This corresponds to the disappearance of the absorbance peak in the 500−600 nm range. An isosbestic point is observed near 500 nm because of the

(30) Connelly, N. G.; Geiger, W. E. *Chem. Rev.* **1996**, *96*, 877–910.
(31) The potential of ferrocene in $MeCN/NBu_4PF_6$ is +0.40 V vs SCE, and SCE is at +0.24 V vs NHE.
(32) Vela, J.; Cirera, J.; Smith, J. M.; Lachicotte, R. J.; Flaschenriem, C. J.; Alvarez, S.; Holland, P. L. *Inorg. Chem.* **2007**, *46*, 60–71.

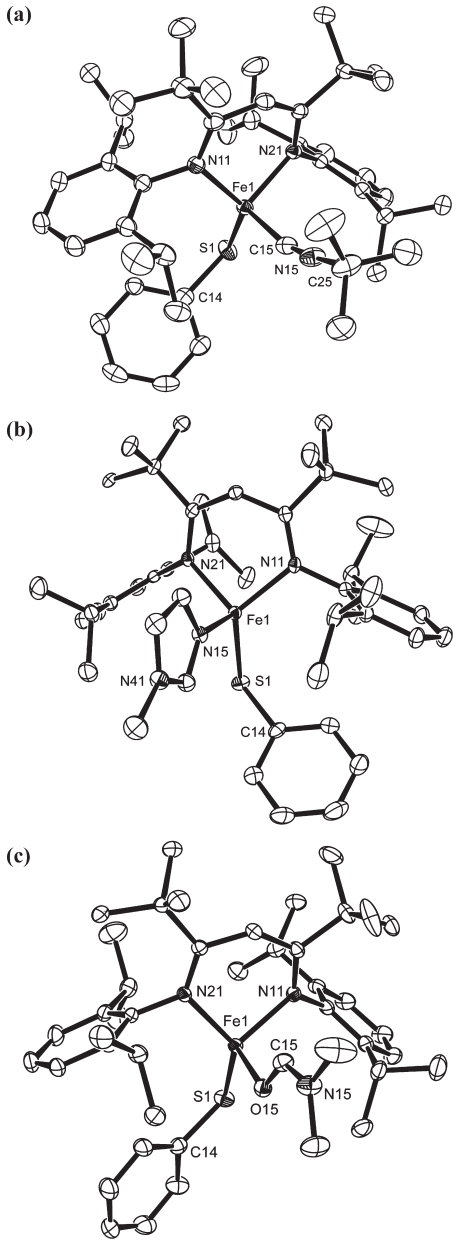


**Figure 4.** ORTEP drawings of the molecular structures of (a) $L^{tBu,iPr2}Fe(SPh)(CN^tBu)$, (b) $L^{tBu,iPr2}Fe(SPh)(MeIm)$ and, (c) $L^{tBu,iPr2}Fe(SPh)(DMF)$. Thermal ellipsoids are shown at 50% probability. Co-crystallized solvent in the $L^{tBu,iPr2}Fe(SPh)(MeIm)$ structure, and all hydrogen atoms, are omitted for clarity.

**Table 3.** Important Bond Distances and Angles for the Four-Coordinate Fe(II) Complexes[a]

| bond/angle | $CN^tBu$ | MeIm | DMF |
|---|---|---|---|
| Fe−N (Å) | 2.000(2), 2.013(2) | 2.021(2), 2.0262(19) | 2.0181(11), 2.0212(11) |
| Fe−S (Å) | 2.2776(15) | 2.2955(11) | 2.2877(4) |
| Fe−L (Å) | 2.089(2) | 2.094(2) | 2.0832(10) |
| N−Fe−N (deg) | 96.19(5) | 96.85(8) | 95.44(4) |
| S−Fe−L (deg) | 118.04(7) | 125.58(6) | 110.31(3) |
| Fe−S−L (deg) | 104.36(6) | 107.05(8) | 112.94(5) |

[a] L represents the fourth donor atom (C, N, or O).

growth of a shoulder in the four-coordinate complex around 400 nm (see Supporting Information). Equilibrium is immediately established between the three-coordinate complex (M) and the four-coordinate complex (ML) in solution (eq 1) upon addition of **L**. The equilibrium constant ($K_{eq}$) can be represented as shown in eqs 1 and 2.

$$M + L \overset{K_{eq}}{\rightleftharpoons} ML \tag{1}$$

$$K_{eq} = \frac{[ML]}{[M][L]} \tag{2}$$

While no clear absorbance band is associated with the four-coordinate complex, its concentration can be calculated from the loss of absorbance ($\Delta A_{\lambda max}$) of the distinct peak of the three-coordinate complex near 550 nm with addition of L. The value of $\Delta A_{\lambda max}$ is plotted against the initial concentration of ligand added, $[L]_0$, to produce a binding curve (Figure 5). Data were only used if an isosbestic point was observed.

The equilibrium constant ($K_{eq}$) is determined by fitting the binding curves to one of two equations depending on whether the ligands bind weakly or strongly to $L^{tBu,iPr2}FeY$. A ligand that binds most of the iron at 1 equiv of L is defined as being "strong binding." Ligands that show less than one-half binding of iron at 1 equiv are considered "weak binding."

In the weak binding scenario, the concentration of ML at equilibrium can be represented by taking the difference of initial and final concentration of M ($[ML] = [M]_0 - [M]_f$). This can be incorporated into an equation to fit a binding curve (eq 3).

$$\frac{[ML]}{[M]_0} = \frac{K_{eq}[L]_0}{K_{eq}[L]_0 + 1} \tag{3}$$

In eq 3, $[L]_0$ is substituted for [L] because in the weak binding situation the concentration of free ligand at equilibrium [L] is virtually identical to the initial concentration of ligand $[L]_0$. However, this assumption is not valid under strong binding conditions. Therefore, eq 4 was formulated taking into account this difference.

$$[ML] = \frac{\left([M]_0 + [L]_0 + \frac{1}{K_{eq}}\right) - \left\{\left([M]_0 + [L]_0 + \frac{1}{K_{eq}}\right)^2 - 4[L]_0[M]_0\right\}^{1/2}}{2} \tag{4}$$

For these experiments, we were interested in learning about the dependence of the binding constant on (a) the type of neutral donor ligand L, and (b) the nature of the spectator ligand Y. To address point (a), a number of representative ligands L were chosen with different donor atoms, steric size, and electronic properties. The values of $K_{eq}$ were determined for binding to both $L^{tBu,iPr2}FeCl$ and to $L^{tBu,iPr2}Fe(SPh)$, to ensure that any trends seen were not peculiar to a single choice of Y. To address point (b), two of the ligands (zMeCN and DMF) were evaluated across a broader range of supporting ligands Y, including the phenolate complex and the $CF_3$-substituted thiophenolate complex.

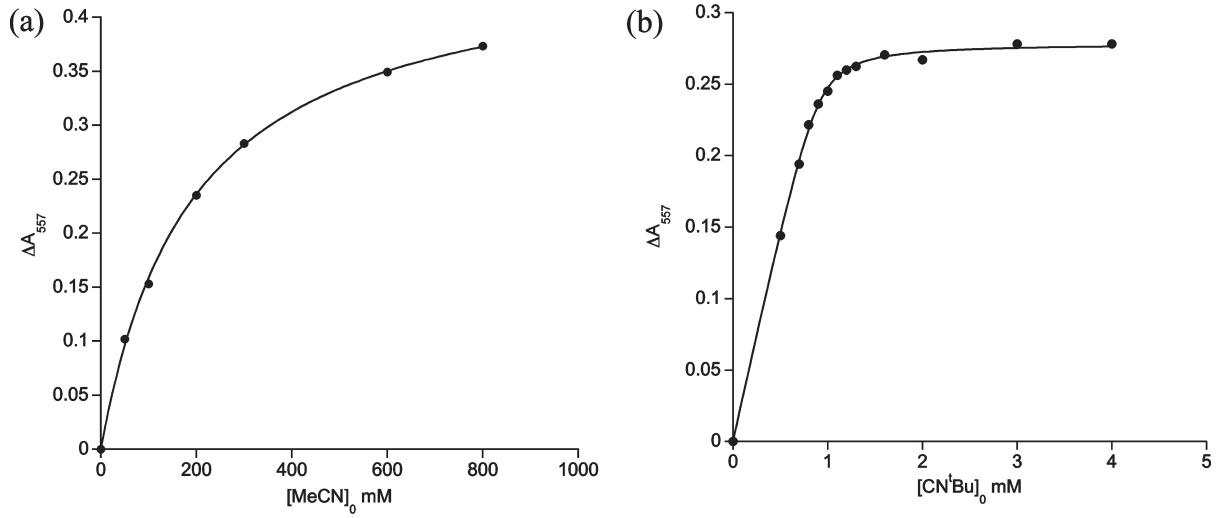


**Figure 5.** Binding curves for (a) $L^{tBu,iPr2}$FeSPh to acetonitrile, an example of weak binding, and (b) $L^{tBu,iPr2}$FeSPh to $CN^tBu$, an example of strong binding.

**Table 4.** Calculated Binding Constants for Neutral Ligands to $L^{tBu,iPr2}$FeCl, $L^{tBu,iPr2}$Fe(SPh), $L^{tBu,iPr2}$Fe(SPhCF$_3$), and $L^{tBu,iPr2}$Fe(OPh)

| ligand | $L^{tBu,iPr2}$FeCl $K_{eq}$ | $L^{tBu,iPr2}$Fe(SPh) $K_{eq}$ | $K_{eq}$(Cl)/$K_{eq}$(SPh) | $L^{tBu,iPr2}$Fe(SPhCF$_3$) $K_{eq}$ | $L^{tBu,iPr2}$Fe(OPh) $K_{eq}$ | donor atom |
|---|---|---|---|---|---|---|
| $PPh_3$ | 0.70 ± 0.08 | 1.0 ± 0.5 | 0.7 ± 0.5 | | | P |
| THF | 0.80 ± 0.01 | 0.15 ± 0.01 | 5.3 ± 0.1 | | | O |
| MeCN | 9.8 ± 0.5 | 5.2 ± 0.2 | 1.9 ± 0.1 | 11.7 ± 0.9 | 4.7 ± 0.4 | N |
| DMF | 390 ± 20 | 160 ± 5 | 2.4 ± 0.1 | 230 ± 10 | 160 ± 10 | O |
| 2-picoline | 660 ± 50 | 300 ± 30 | 2.2 ± 0.1 | | | N |
| Pyridine | 41000 ± 6000 | 11000 ± 2000 | 3.7 ± 0.3 | | | N |
| $CN^tBu$ | 73000 ± 27000 | 41000 ± 7000 | 1.8 ± 0.7 | | | C |

Irrespective of Y, added ligands $PPh_3$, THF, MeCN, DMF, and 2-picoline were appropriate for use of the "weak binding" equation (eq 3) and exhibited $K_{eq}$ values between $10^{-1}$ to $10^3$. Pyridine and $CN^tBu$ were fitted with the "strong binding" equation (eq 4) and were associated with $K_{eq}$ values above $10^4$. These data are summarized in Table 4.

The values of $K_{eq}$ are highly dependent on the neutral ligand L. However, the $K_{eq}$ values are similar with the same added ligand L and different anionic ligands Y. Equivalently, the trends of L binding are similar no matter which Y is used. The similarity in the trends is most evident when comparing $K_{eq}$ values of $L^{tBu,iPr2}$FeCl and $L^{tBu,iPr2}$Fe(SPh), where the $K_{eq}$ values for $L^{tBu,iPr2}$-FeCl are approximately twice that of $L^{tBu,iPr2}$Fe(SPh).

## Discussion

**Three-Coordinate Iron(II) Thiolate Complexes.** The three $L^{tBu,iPr2}$FeSAr complexes described here add to the few examples of three-coordinate iron thiolate complexes. The most common S-coordinated iron complexes with a coordination number of three are $Fe_2(\mu\text{-SR})_2$ dimers.[33−38] Previous three-coordinate iron thiolates have extremely bulky ligands that enable them to resist the tendency of thiolates to bridge between metals.[13,28,36,39,40] The SR group in most such literature compounds is a substituted thiophenolate with bulky *tert*-butyl groups in the ortho- and para-positions. Here, on the other hand, the use of a bulky $\beta$-diketiminate ligand enables the use of smaller thiolates.

**Binding of Neutral Ligands to Low-Coordinate Iron.** In this paper we report the binding constants for a range of ligands to low-coordinate Fe(II) complexes, determined using UV−vis spectroscopy. Binding of the added donor ligand is instantaneous as observed by the immediate color change of the solution. Crystal structures show that the ligand binds to $L^{tBu,iPr2}$FeY in a 1:1 stoichiometry. The 1:1 binding is further supported by the observation of an isosbestic point when comparing samples at different concentrations of added ligand (see Supporting Information, Figures S3−S6 for examples).

The measured values of $K_{eq}$ varied greatly with variation of the neutral ligand but were independent of the donor atom and hybridization of the donor atom in the neutral ligand. In an effort to discern what factors were responsible for the observed trend, we explored both steric and electronic explanations in a systematic fashion.

**Steric Effect of Ligands.** Steric contributions were surveyed by calculating the cone and solid angles of the fourth donor ligands. The more familiar cone angle ($\theta$), as

(33) Ohki, Y.; Ikagawa, Y.; Tatsumi, K. *J. Am. Chem. Soc.* **2007**, *129*, 10457–10465.
(34) Ohta, S.; Ohki, Y.; Ikagawa, Y.; Suizu, R.; Tatsumi, K. *J. Organomet. Chem.* **2007**, *692*, 4792–4799.
(35) Power, P. P.; Shoner, S. C. *Angew. Chem.* **1991**, *103*, 308−309 (See also *Angew. Chem., Int. Ed. Engl.* **1991**, *30*(3), 330−332).
(36) Hauptmann, R.; Kliss, R.; Schneider, J.; Henkel, G. *Z. Anorg. Allg. Chem.* **1998**, *624*, 1927–1936.
(37) Ruhlandt-Senge, K.; Power, P. P. *Bull. Soc. Chim. Fr.* **1992**, *129*, 594.
(38) Sydora, O. L.; Henry, T. P.; Wolczanski, P. T.; Lobkovsky, E. B.; Rumberger, E.; Hendrickson, N. H. *Inorg. Chem.* **2006**, *45*, 609–626.
(39) Lee, H. K.; Luo, B.-S.; Mak, T. C. W.; Leung, W.-P. *J. Organomet. Chem.* **1995**, *489*, C71–C73.
(40) Groysman, S.; Wang, J.-J.; Tagore, R.; Lee, S. C.; Holm, R. H. *J. Am. Chem. Soc.* **2008**, *130*, 12794–12807.

described by Tolman,[41] describes the amount of space a ligand occupies by measuring the angle created at the apex of a cone that completely contains the ligand (Figure 6a). The concept of a solid angle (Ω) is less familiar, but is perhaps a more accurate way to represent the steric congestion of a ligand by taking the ligand's shape into account. It is measured in steradians and represented by eq 5 where $A$ is the area of a circle created on a sphere if a light is shone on the ligand from a metal located at the center of the sphere (Figure 6b).

$$\Omega = \frac{A}{r^2} \tag{5}$$

The cone angles and solid angles for ligands of interest were calculated using the program SolidG, provided by Ilia Guzei.[42] For each ligand, we chose 10 representative structures (listed in the Supporting Information) containing the ligand of interest in the CSD. The values for each ligand were calculated and averaged to give the values shown in Table 5.

Despite a variety of spectator ligands in the reference complexes (see Supporting Information for full lists of reference complexes), there was little variation in the derived cone angle and solid angle values for the same target ligand. A further non-systematic survey confirmed that the coordination number and metal type do not significantly affect the cone and solid angle calculated for a given ligand. In addition, the cone angle and solid angle correlate quite well with one another. So, these values are likely to be accurate representations of the relative amount of steric hindrance caused by each of these ligands in the four-coordinate complexes $L^{tBu,iPr2}Fe(Y)(L)$.

The size of most ligands was similar: aside from 2-picoline and triphenylphosphine, the solid angles varied in the narrow range 1.60 to 1.90. Given the wide variation in $K_{eq}$ between the ligands of similar size, it is clear that steric effects are not dominant in this system. However, the two largest ligands are insightful. 2-Picoline was chosen as a ligand that is electronically similar to pyridine but is substantially larger (solid angle of 2.36 vs 1.90). The added size reduces the binding constant by a factor of 30−60. In addition, the bulkiest ligand, $PPh_3$, was the most weakly binding. Overall, steric effects have an influence on $K_{eq}$ for 2-picoline and $PPh_3$ but do not explain the trends with the other neutral ligands.

**Electronic Properties of Ligands: σ-Effects.** To rationalize the σ-bonding capacity of different ligands, we compared the binding constants to the gas-phase proton affinities of ligands, as well as the p$K_a$ of their conjugate acids. We were not able to find a literature value for the p$K_a$ of protonated *t*-butyl isocyanide in MeCN, and so it was calculated using a recently reported semiempirical density functional theory (DFT) method.[43] The relevant values are shown in Table 6.

No correlation was found between $K_{eq}$ and the proton affinities. There was a weak correlation of $K_{eq}$ with the p$K_a$ values if $CN^tBu$ and the bulky ligands are left out (Figure 7). Therefore, the ligands that bind most tightly to a proton also bind most tightly to the iron atom.

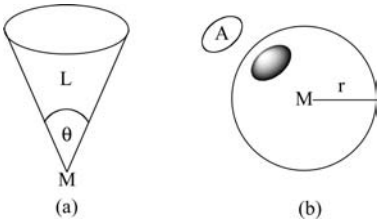


**Figure 6.** Graphical representations of a cone angle (a) and solid angle (b).

**Table 5.** Calculated Solid and Cone Angles of Ligands Used in This Study

| ligand | solid ang (Ω) | cone ang (θ) | $K_{eq}$(Cl) |
|---|---|---|---|
| $PPh_3$ | 3.32(6) | 124(1) | 0.70 |
| THF | 1.81(6) | 89(2) | 0.80 |
| MeCN | 1.60(0) | 83.69(3) | 9.80 |
| DMF | 1.63(4) | 85(1) | 390 |
| 2-Picoline | 2.36(3) | 102.8(6) | 660 |
| Pyridine | 1.90(2) | 91.6(5) | 41000 |
| $CN^tBu$ | 1.65(1) | 85.0(3) | 90000 |

However, the large deviation of the isocyanide indicates that σ-effects are not the sole explanation for the electronic effects on $K_{eq}$.

**Electronic Properties of Ligands: π-Effects.** *t*-Butyl isocyanide is the strongest π-acceptor ligand studied here and has the largest equilibrium constant, suggesting that π-backbonding might account for the remaining deviation from the trends discussed above. Previous binding studies of low-coordinate iron(I) to alkynes and alkenes showed that π-backbonding was the dominant factor determining the affinity of different ligands.[44] A very recent computational study has found that the binding constants in iridium systems can be related to backbonding. [45]

Out of the ligands studied, the ability to accept electron density is greatest for $CN^tBu$.[46] Low-lying unoccupied molecular orbitals (LUMOs) are also present in pyridine and $PPh_3$, but in the last case the great steric hindrance of the phenyl groups on the phosphine prevents this ligand from binding strongly. In attempts to quantitatively compare the π-backbonding ability of these ligands, the carbonyl stretch values of tungsten pentacarbonyl complexes ($W(CO)_5L$) containing the ligand of interest were collected (see Table 7). Unfortunately, there was no evident correlation between this measure of backbonding ability and the equilibrium constant for binding to three-coordinate iron.

To further test the importance of π-backbonding, $L^{tBu,iPr2}FeCl$ and $L^{tBu,iPr2}FeSPh$ were each treated with 1 atm of CO under a range of conditions. However, these reactions yielded starting material, decomposition products, or diamagnetic products as observed by $^1H$ NMR. Infrared spectroscopy of these reactions showed no absorbances from 1700−2600 $cm^{-1}$ where C−O stretches of β-diketiminate iron(I) and iron(II) carbonyl compounds have been observed.[10,47,48] Therefore, if CO binds

(41) Tolman, C. A. *Chem. Rev.* **1977**, *77*, 313–348.
(42) Guzei, I. A.; Wendt, M. *Dalton Trans.* **2006**, 3991–3999.
(43) Ding, F.; Smith, J. M.; Wang, H. J. *J. Org. Chem.* **2009**, *74*, 2679–2691.
(44) Yu, Y.; Smith, J. M.; Flaschenriem, C. J.; Holland, P. L. *Inorg. Chem.* **2006**, *45*, 5742–5751.
(45) Gusev, D. G. *Organometallics* **2009**, *28*, 763–770.
(46) Barbeau, C.; Turcotte, J. *Can. J. Chem.* **1976**, *54*, 1603–1611.
(47) Smith, J. M.; Lachicotte, R. J.; Holland, P. L. *Organometallics* **2002**, *21*, 4808–4814.
(48) Sadique, A. R.; Brennessel, W. W.; Holland, P. L. *Inorg. Chem.* **2008**, *47*, 784–786.

**Table 6.** $H^+$ Affinity Values and $pK_a$ Values in MeCN for the Ligands Studied

| ligand | $H^+$ affinity[a] (kJ/mol) | $pK_a$ (MeCN) | $K_{eq}$(Cl) |
|---|---|---|---|
| $PPh_3$ | 972.8 | 7.61[b] | 0.7 |
| THF | 822.1 | 1.1[c] | 0.8 |
| MeCN | 779.2 | 0 | 9.8 |
| DMF | 887.5 | 6.1[c] | 390 |
| 2-picoline | 949.1 | 13.32[c] | 660 |
| Pyridine | 930 | 12.53[b] | 41000 |
| $CN^tBu$ | 870.7 | 2.71[d] | 90000 |

[a] Hunter, E. P.; *J. Phys. Chem.* **1998**, 27, 3991−3999. [b] Kaljurand, I.; Kütt, A.; Sooväli, L.; Rodima, T.; Mäemets, V.; Leito, I.; Koppel, I. A. *J. Org. Chem.* **2005**, *70*, 1019−1028. [c] Izutsu, K. *Acid−Base Dissociation Constants in Dipolar Aprotic Solvents*; Blackwell Scientific: Oxford, 1990, pp 17−35. [d] Calculated: see ref 43 and Experimental Section.

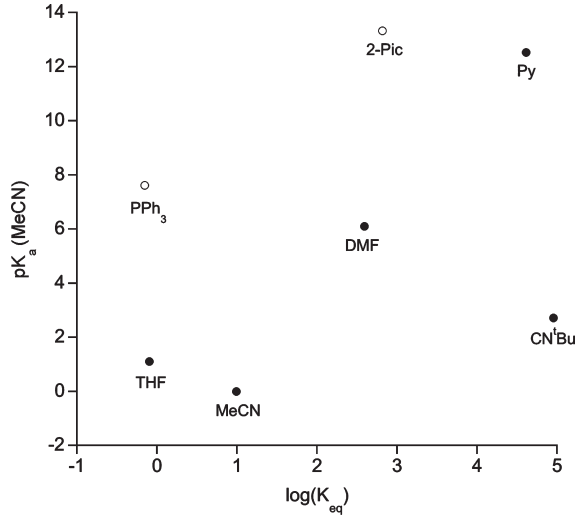


**Figure 7.** Plot of $\log(K_{eq})$ vs $pK_a$ (MeCN) for different ligands L. As discussed above, $PPh_3$ and 2-picoline fall from the trend because of steric congestion in $PPh_3$ and 2-picoline (Table 5). The deviation of $CN^tBu$ may be attributable to $\pi$-backbonding (see below).

at all to the three-coordinate iron complexes, it is a very weak interaction. Note that related three-coordinate iron-alkyl complexes react with CO to give a low-spin iron-acyl product from CO insertion, so weak CO interactions must be possible in some three-coordinate iron(II) compounds.[47]

Therefore, despite a likely influence of $\pi$-backbonding in isocyanide complexes, it is not the dominant factor either. Overall, the trends in the binding strength of neutral ligands are determined by a combination of steric and electronic effects, none of which dominates.

**Steric and Electronic Effects from the Spectator Ligand Y.** As noted above, there was a small increase in binding constants of neutral ligands to $L^{tBu,iPr2}FeCl$ as compared to the binding constants to $L^{tBu,iPr2}FeSPh$. One could reasonably attribute this difference to electronic effects (the greater electronegativity of chlorine vs sulfur), or to steric effects (the smaller size of chlorine vs sulfur). Even though the effect was small, we took this opportunity to compare the binding constants with two additional complexes: one with an electron-withdrawing substituent on the arylthiolate, $L^{tBu,iPr2}Fe(SC_6H_4CF_3)$, and one with oxygen in place of sulfur, $L^{tBu,iPr2}Fe(OPh)$. Both of these ligands are nearly isosteric with the arylthiolate ligand in $L^{tBu,iPr2}FeSPh$.

**Table 7.** Collected CO Stretch Values ($cm^{-1}$) of $W(CO)_5L$

| $W(CO)_5L$ | $A_1$ | $A_1$ | E | $K_{eq}$(Cl) |
|---|---|---|---|---|
| $PPh_3$[a] | 2072 | 1942 | 1939 | 0.7 |
| THF[b] | 2074 | 1912 | 1933 | 0.8 |
| MeCN[c] | 2083 | 1931 | 1948 | 9.8 |
| DMF[c] | 2067 | 1847 | 1917 | 390 |
| Pyridine[d] | 2076 | 1980 | | 41000 |
| $CN^tBu$[e] | 2065 | 1922 | 1952 | 90000 |

[a] Bancroft, G. M.; Dignard-Bailey, L.; Puddephatt, R. J. *Inorg. Chem.* **1986**, *25*, 3675−3680. [b] We substituted the value known for dihydrofuran: Paur-Afshari, R.; Lin, J.; Schultz, R. H. *Organometallics* **2000**, *19*, 1682−1691. [c] Stolz, I. W.; Dobson, G. R.; Sheline, R. K. *Inorg. Chem.* **1963**, *2*, 323−326. [d] Kraihanzel, C. S.; Cotton, F. A. *Inorg. Chem.* **1963**, *2*, 533−540. [e] King, R. B.; Saran, M. S. *Inorg. Chem.* **1974**, *13*, 74−78.

Because the binding constants are most precise with weak-binding ligands, we used MeCN and DMF as added neutral donors across the range of spectator ligands Y. The binding curves using $L^{tBu,iPr2}Fe(OPh)$ and $L^{tBu,iPr2}Fe(SPhCF_3)$ yielded $K_{eq}$ values that were similar to the chloride and thiophenolate complexes (see Table 4 above). No clear trends are discernible, casting doubt on an electronic explanation for the small difference between binding to thiolate and to chloride complexes.

We also attempted to evaluate the electronic effect of Y on the complex using cyclic voltammetry (CV) to determine the reduction potential (the oxidations were irreversible). These studies were performed in both $Et_2O$, to evaluate the three-coordinate species, and MeCN, to evaluate the four-coordinate species. The $Fe^{2+/1+}$ waves were more reversible in $Et_2O$ than MeCN. This may indicate greater stability of the three-coordinate iron(I) species than the four-coordinate iron(I) species. Only small variations in potential ($< 200$ mV) are observed upon changing the anionic ligand Y. In the two solvents, these small shifts follow opposite trends. For example, $L^{tBu,iPr2}Fe(OPh)$ has the most negative reduction potential in $Et_2O$, while $L^{tBu,iPr2}Fe(OPh)(NCMe)$ has the least negative reduction potential value in MeCN. The reduction potentials appear to be roughly 150 mV less negative in MeCN than in $Et_2O$. However, because the waves in MeCN are quasireversible, it would be dangerous to draw any conclusion from this trend. Overall, the similarity of the potentials with different Y suggests that the electronegativity of the third donor does not significantly influence the electronic properties of the metal center.

**Implications for Modeling Nitrogenase.** As described in the Introduction, our group has used diketiminate complexes as mimics of one- and two-iron "belt" sites on nitrogenase.[6] This has naturally raised questions about the use of nitrogen donors to mimic a sulfur-coordinated iron site. In this study, the diketiminate was not varied, but one of the ligands was systematically changed over a range from "hard" oxygen and chlorine ligands to "soft" thiolate. This enabled us to experimentally gauge the influence of changing one spectator ligand on the binding ability and other properties of a three-coordinate iron complex.

In this context, it is interesting that the binding constants for a variety of neutral ligands are similar with oxygen, sulfur, or chloride spectator ligands in one

position. This similarity was evident with neutral ligands that are $\pi$-donors (e.g., THF) or $\pi$-acceptors (e.g., $CN^tBu$). The reduction potentials of the iron(II) complexes were also similar over the range of spectator ligands. This insensitivity to the spectator ligand suggests that changes in donor, such as from diketiminates to thiolates or sulfides, may give only a small influence on binding energies and redox potentials. Of course, in the broader field of coordination chemistry, the identity of spectator ligands often influences binding energies and mechanisms;[49,50] however, in the three-coordinate systems studied here, the effects of changing one ligand are surprisingly small.

In recent publications, Holland[15] and Peters[51] have explored geometric influences on the unusual electronic structures and reactivity of high-spin, late-metal complexes with three or four ligands, respectively. These works show that the geometry of the metal has a pronounced effect on its electronic structure, and it is likely that the geometric influences are much more important than the precise electronics of the spectator ligand in determining the properties of the resulting complex. Further systematic studies are needed to evaluate the influence of geometry on measurable chemical parameters like binding constants.

## Experimental Section

**Synthetic Methods.** All manipulations were performed under a nitrogen atmosphere by standard Schlenk techniques or in an M. Braun glovebox maintained at or below 1 ppm of $O_2$ and $H_2O$. Glassware was dried at 150 °C overnight. $^1H$ NMR data were recorded on a Bruker Avance 500 spectrometer (500 MHz) at 22 °C and referenced internally to residual protiated solvent ($C_6HD_5$ at $\delta$ 7.16 ppm). Peaks of these paramagnetic complexes are all singlets. Relative integrations of peaks and assignments are given except for the four-coordinate complexes, where overlap of peaks is too great to integrate accurately. Solution magnetic susceptibilities were determined at 294 K using Evans' method.[25,26] Electronic spectra were recorded between 400 and 800 nm on a Cary 50 UV−visible spectrophotometer, using screw-cap quartz cuvettes of 1 cm optical path length. Elemental analyses were performed by the Microanalysis Laboratory at the University of Illinois (Urbana, Illinois) or Columbia Analytical Services (Tucson, AZ). Infrared spectra (600−4000 $cm^{-1}$) were recorded on KBr pellets in a Shimadzu FTIR spectrophotometer (FTIR-8400S).

Acetonitrile, pentane, diethyl ether, THF, and toluene were purified by passage through activated alumina and "deoxygenizer" columns obtained from Glass Contour Co. DMF was dried over 3 Å molecular sieves. Deuterated benzene was dried over activated alumina in a bomb flask, and the alumina was filtered off into a storage container prior to use. Before use, an aliquot of each solvent (except acetonitrile) was tested with a drop of sodium benzophenone ketyl in THF solution. Celite and alumina were dried overnight at 200 °C under vacuum. $FeCl_2(THF)_{1.5}$ was synthesized by the method of Kern.[52] $KL^{tBu,iPr2}$ was synthesized by adding benzylpotassium[22] to $HL^{tBu,iPr2}$ in diethyl ether.[23]

CV measurements were obtained using a Cypress Systems 3100 potentiostat. The working electrode was glassy carbon with a 1 mm diameter working area, and Ag wires were used as auxiliary and reference electrodes. All measurements were referenced with an internal ferrocene standard, and reported relative to the $Cp_2Fe^+/Cp_2Fe$ couple. Acetonitrile used for CV experiments was vacuum transferred after alumina treatment.

**X-ray Crystallography.** Single crystals were mounted on a glass capillary tube or fiber and mounted on a Siemens SMART CCD or Bruker SMART APEX II CCD Platform diffractometer for data collection under a cold $N_2$ stream at 193(2) K or 100.0(1) K. Full data collection was carried out using Mo K$\alpha$ radiation (graphite monocromator) with appropriate frame times ranging from 20 to 90 s and typical detector distance around 5.09 cm. Total data collection time was generally between 12 and 24 h. Structures were refined using SIR97 or SHELXS-97 and refined using SHELXL-97 (Table 8). Space groups were determined based on systematic absences and intensity statistics. A direct-methods solution was calculated which provided most non-hydrogen atoms from the E-map. Full-matrix least-squares/difference Fourier cycles were performed which located the remaining non-hydrogen atoms. All non-hydrogen atoms were refined with anisotropic displacement parameters. All hydrogen atoms were placed in ideal positions and refined as riding atoms with relative isotropic displacement parameters.

**Modified Procedure for $L^{tBu,iPr2}FeCl$[21].** Under an atmosphere of $N_2$, $KL^{tBu,iPr2}$ (0.50 g, 0.92 mmol), $FeCl_2(THF)_{1.5}$ (0.202 g, 0.919 mmol), and toluene (25 mL) were added to a 150 mL resealable tube. The mixture was heated in an oil bath at 100 °C for 18 h and turned very dark red in color. The solution was cooled, filtered through Celite, and concentrated to 7 mL. The solution was warmed to dissolve a small amount of solid formed during concentration, and cooled to −40 °C overnight to afford dark red crystals. The supernatant was decanted and the red solid was washed with 1 mL of pentane to remove trace $L^{tBu,iPr2}H$, leaving $L^{tBu,iPr2}FeCl$ (0.531 g, 97%). $^1H$ NMR ($C_6D_6$, 500 MHz): $\delta$ 104 (s, 1H, α-H), 42 (s, 18H, tBu), 2.6 (s, 4H, *m*-aryl), −27 (s, 12H, *i*Pr methyl), −108 (s, 4H, *i*Pr methine), −111 (s, 12H, *i*Pr methyl), −115 (s, 2H, *p*-aryl). Occasionally, trace water gives up to 5% of $L^{tBu,iPr}H$, which is observed as a white solid, or as peaks at 1−2 ppm of the $^1H$ NMR spectrum. The most reliable way to gauge purity is UV−visible spectroscopy in toluene ($\lambda_{max}$ = 559 nm; $\varepsilon$ = 63(3) $M^{-1}$ $cm^{-1}$).

**$L^{tBu,iPr2}Fe(Y)$ (Y = SPh, STol, $SPhCF_3$, OPh, OTol).** The appropriate thiophenol or phenol was treated with a slight excess of NaH (1.05 equiv), and stirred in THF for 2 h. The solution was filtered through Celite, and solvent was removed under vacuum.

To a stirring solution of $L^{tBu,iPr2}FeCl$ (0.0593 g, 0.100 mmol) in $Et_2O$ (5−10 mL) was added 1.0 equiv of the appropriate sodium salt. The resulting orange colored solution and suspension was stirred for 2 h. The solvent was evaporated under vacuum, and the residue was extracted with pentane (10 mL) and filtered through Celite to give a clear red-orange solution. This solution was concentrated to 5 mL, warmed briefly to achieve a homogeneous solution, cooled and placed in a freezer (−35 °C) to afford red-orange crystals. Specific yields are given below.

**$L^{tBu,iPr2}Fe(SPh)$.** Yield 80%. $^1H$ NMR ($C_6D_6$, 500 MHz): $\delta$ 87 (1H, α-H), 56 (2H, *o*-SPh), 50 (2H, *m*-SPh), 40 (18H, tBu), 6.1 (4H, *m*-Ar), −7.6 (1H, *p*-SPh), −24 (12H, *i*Pr methyl), −99 (4H, *i*Pr methine), −112 (12H, *i*Pr methyl), −114 (2H, *p*-Ar) ppm. $\mu_{eff}$ (Evans, $C_6D_6$): 5.1(5) $\mu_B$. UV−vis (Tol) $\lambda_{max}$: 550 nm (51(3) $M^{-1}$ $cm^{-1}$). IR (KBr): 2960 (s), 2870 (m),

(49) Bryndza, H. E.; Domaille, P. J.; Paciello, R. A.; Bercaw, J. E. *Organometallics* **1989**, *8*, 379–385.
(50) Henderson, R. A. *Chem. Rev.* **2005**, *105*, 2365−2437. In [4Fe-4S] clusters, changing from terminal chloride to thiolate ligands has been reported to change the substitution mechanism from associative to dissociative.
(51) Jenkins, D. M.; Peters, J. C. *J. Am. Chem. Soc.* **2005**, *127*, 7148–7165.
(52) Kern, R. J. *J. Inorg. Nucl. Chem.* **1962**, *24*, 1105–1109.

**Table 8.** X-ray Structure Parameters for the Three- And Four-Coordinate Complexes Discussed in This Work

| | $L^{tBu,iPr2}Fe$ (SPh) | $L^{tBu,iPr2}Fe$ ($SPhCF_3$) | $L^{tBu,iPr2}Fe$ (STol) | $L^{tBu,iPr2}Fe$ (OTol) | $L^{tBu,iPr2}Fe(SPh)$ ($CN^tBu$) | $L^{tBu,iPr2}Fe(SPh)$ (MeIm)·$C_6H_6$ | $L^{tBu,iPr2}Fe(SPh)$ (DMF) |
|---|---|---|---|---|---|---|---|
| empirical formula | $C_{41}H_{58}N_2SFe$ | $C_{42}H_{57}N_2F_3SFe$ | $C_{42}H_{60}N_2SFe$ | $C_{42}H_{60}N_2OFe$ | $C_{46}H_{67}N_{3S}SFe$ | $C_{51}H_{70}N_4SFe$ | $C_{44}H_{65}N_3OSFe$ |
| fw | 666.8 | 734.81 | 680.83 | 664.77 | 749.94 | 827.02 | 739.9 |
| temperature (K) | 193(2) | 193(2) | 193(2) | 193(2) | 100.0(1) | 100.0(1) | 100.0(1) |
| cryst system | monoclinic | monoclinic | monoclinic | monoclinic | monoclinic | triclinic | triclinic |
| space group | $P2_1/n$ | $P2_1/c$ | $P2_1/c$ | $P2_1/c$ | $P2_1/n$ | $P\bar{1}$ | $P\bar{1}$ |
| $a$ (Å) | 10.8405(15) | 22.1226(10) | 22.1137(11) | 22.0892(14) | 10.693(9) | 9.575(5) | 10.3921(12) |
| $b$ (Å) | 16.368(2) | 9.6586(4) | 9.6346(5) | 9.6154(6) | 19.719(16) | 12.487(5) | 12.4143(14) |
| $c$ (Å) | 21.579(3) | 20.9138(9) | 20.4372(10) | 20.5038(13) | 21.014(17) | 20.562(5) | 17.392(2) |
| | | | | | 90 | 79.982(5) | 102.907(2) |
| $\beta$ (deg) | 91.007(2) | 114.980(1) | 114.858(1) | 115.819(1) | 96.683(12) | 77.463(5) | 99.220(2) |
| | | | | | 90 | 88.120(5) | 94.130(2) |
| $V$ (Å$^3$) | 3828.3(9) | 4050.7(3) | 3950.9(3) | 3920.2(4) | 4401(6) | 2363.2(17) | 2145.2(4) |
| $Z$ | 4 | 4 | 4 | 4 | 4 | 2 | 2 |
| $\rho$ (g/cm$^3$) | 1.157 | 1.205 | 1.145 | 1.126 | 1.132 | 1.162 | 1.145 |
| $\mu$ (mm$^{-1}$) | 0.477 | 0.468 | 0.464 | 0.147 | 0.423 | 0.400 | 0.434 |
| R1 | 0.0420 | 0.0344 | 0.0377 | 0.0534 | 0.0489 | 0.0562 | 0.0431 |
| wR2 [$I > 2\sigma(I)$] | 0.1012 | 0.0946 | 0.0897 | 0.1114 | 0.1113 | 0.1016 | 0.0949 |
| GOF | 1.017 | 1.087 | 1.039 | 1.058 | 1.018 | 0.975 | 1.010 |

1624(w), 1577 (w), 1502 (m), 1473 (w), 1459 (w), 1430 (s), 1375 (m), 1354 (s), 1317 (m), 1217 (w), 1096 (w), 1024 (w), 780 (w), 736 (m), 697 (w) cm$^{-1}$ Anal. Calcd for $C_{41}H_{58}N_2SFe$: C, 73.84; H, 8.76; N, 4.20%. Found: C, 74.20; H, 9.01; N, 4.27%.

**$L^{tBu,iPr2}Fe(STol)$.** Yield 75%. $^1$H NMR ($C_6D_6$, 500 MHz): $\delta$ 87 (1H, α-H), 54 (2H, *o*-STol), 50 (2H, *m*-STol), 45 (3H, $CH_3$−STol), 40 (18H, tBu), 5.9 (4H, *m*-Ar), −24 (12H, *i*Pr methyl), −99 (4H, *i*Pr methine), −111 (12H, *i*Pr methyl), −114 (2H, *p*-Ar) ppm. UV−vis (Tol.) $\lambda_{max}$: 553 nm (45(2) M$^{-1}$ cm$^{-1}$). IR (KBr, cm$^{-1}$): 2963 (s), 2867 (m), 1624 (m), 1535 (w), 1503 (m), 1485 (m), 1458 (m), 1430 (m), 1375 (m), 1355 (s), 1316 (m), 1218 (w), 1108 (w), 1087 (m), 932 (w), 805 (m), 762 (m). Anal. Calcd for $C_{42}H_{60}N_2SFe$: C, 74.09; H, 8.88; N, 4.11%. Found: C, 73.78; H, 8.84; N, 4.04%.

**$L^{tBu,iPr2}Fe(SPhCF_3)$.** Yield 85%. $^1$H NMR ($C_6D_6$, 500 MHz): $\delta$ 84 (1H, α-H), 54 (2H, *o*-SPh), 49 (2H, *m*-SPh), 40 (18H, tBu), 7.9 (4H, *m*-Ar), −24 (12H, *i*Pr methyl), −98 (4H, *i*Pr methine), −111 (12H, *i*Pr methyl), −118 (2H, *p*-Ar) ppm. $\mu_{eff}$ (Evans, $C_6D_6$): 4.9(5) $\mu_B$. UV−vis (Tol) $\lambda_{max}$: 563 nm (42(2) M$^{-1}$ cm$^{-1}$). IR (KBr cm$^{-1}$): 2964 (s), 2873 (w), 1600 (m), 1503 (m), 1353 (s), 1323 (vs), 1158 (m), 1116 (m), 1091 (m), 1062 (w), 1014 (w), 827 (w), 800 (w), 781 (w). Anal. Calcd for $C_{42}H_{57}N_2SFe$: C, 68.64; H, 7.82; N, 3.81%. Found: C, 68.37; H, 8.09; N, 3.80%.

**$L^{tBu,iPr2}Fe(OPh)$.** Yield 78%. $^1$H NMR ($C_6D_6$, 500 MHz): $\delta$ 119 (1H, α-H), 94 (2H, *o*-OPh), 60 (2H, *m*-OPh), 42 (18H, tBu), −4.4 (4H, *m*-Ar), −7.2 (1H, *p*-OPh), −30 (12H, *i*Pr methyl), −103 (2H, *p*-Ar), −118 (4H, *i*Pr methine, 12H, *i*Pr methyl) ppm. $\mu_{eff}$ (Evans, $C_6D_6$): 5.6(5) $\mu_B$. UV−vis (Tol) $\lambda_{max}$: 533 nm (56(3) M$^{-1}$ cm$^{-1}$). IR (KBr cm$^{-1}$): 2959 (s), 2867 (w), 1588 (m), 1490 (s), 1430 (w), 1376 (m), 1359 (s), 1318 (m), 1294 (m), 1217 (w), 1180 (w), 1096 (w), 871 (w), 802 (w), 755 (m), 691 (w). Anal. Calcd for $C_{41}H_{58}N_2OFe$: C, 75.67; H, 8.98; N, 4.30%. Found: C, 75.29; H, 8.90; N, 4.08%.

**$L^{tBu,iPr2}Fe(OTol)$.** Yield 75%. $^1$H NMR ($C_6D_6$, 400 MHz): $\delta$ 117 (1H, α-H), 94 (2H, *o*-OTol), 83 (3H, $CH_3$−OTol), 55 (2H, *m*-OTol), 41 (18H, tBu), −4.1 (4H, *m*-Ar), −29 (12H, *i*Pr methyl), −101 (2H, *p*-Ar), −115 (4H, *i*Pr methine, 12H, *i*Pr methyl) ppm. UV−vis ($Et_2O$) $\lambda_{max}$: 531 nm (79(4) M$^{-1}$ cm$^{-1}$). IR (KBr cm$^{-1}$): 2963 (s), 2870 (w), 1618 (w), 1502 (s), 1459 (w), 1430 (w), 1360 (s), 1319 (m), 1280 (m), 1105 (w), 934 (w), 873 (w), 821 (m), 779 (w), 762 (m). Anal. Calcd for $C_{42}H_{60}N_2OFe$: C, 75.88; H, 9.09; N, 4.21%. Found: C, 74.83; H, 9.13; N, 4.22%. This compound is somewhat unstable in solution, depositing a solid over time. Therefore, its purity is suspect, consistent with the elemental analysis data.

**$L^{tBu,iPr2}Fe(SPh)(CN^tBu)$.** In a 20 mL scintillation vial, $CN^tBu$ (70 $\mu$L, 0.619 mmol) was added via syringe to a red-orange solution of $L^{tBu,iPr2}Fe(SPh)$ (81.0 mg, 0.122 mmol) in $Et_2O$ (8 mL). The solution was cooled to −35 °C overnight to give orange crystals (67.8 mg, 75%). $^1$H NMR ($C_6D_6$, 500 MHz): $\delta$ 33, 27, 25, 20, 13, 8.1, 4.0, 2.1, 1.2, 0.29, −4.4, −4.9, −17, −50 ppm. IR (KBr): 3057 (w), 2962 (vs), 2868 (m), 2168 (s), 2127 (m), 1618 (m), 1491 (m), 1473 (m), 1465 (w), 1431 (m), 1352 (s), 1315 (s), 1254 (w), 1215 (m), 1153 (w), 1105 (w), 1024 (w), 933 (w), 887 (w), 795 (w), 762 (w), 739 (w), 692 (w) cm$^{-1}$. Anal. Calcd for $C_{46}H_{67}N_3SFe$: C, 73.67; H, 9.00; N, 5.60%. Found: C, 72.87; H, 9.01; N, 5.58%.

**$L^{tBu,iPr2}Fe(SPh)(DMF)$.** In a 20 mL scintillation vial, DMF (94 $\mu$L, 1.21 mmol) was added via syringe to a red-orange solution of $L^{tBu,iPr2}Fe(SPh)$ (81.8 mg, 0.123 mmol) in $Et_2O$ (10 mL). Upon swirling the solution orange crystals began to form. Cooling to −35 °C gave orange crystals in two crops (84.5 mg, 93%). Anal. Calcd for $C_{45}H_{67}N_3OSFe$: C, 71.42; H, 8.85; N, 5.68%. Found: C, 70.66; H, 8.71; N, 5.46%. IR (KBr): 3063(w), 2968 (vs), 2868 (m), 1651 (vs), 1578 (m), 1527 (w), 1487 (m), 1460 (s), 1431 (s), 1383 (s), 1360 (s), 1315 (m), 1251 (w), 1217 (w), 1184 (w), 1153 (w), 1109 (m), 1063 (w), 1024 (w), 933 (w), 885 (w), 794 (w), 764 (m), 739 (m) 692 (m) cm$^{-1}$. $^1$H NMR ($C_6D_6$, 500 MHz): $\delta$ 33, 18.0, 17.6, 5.8, 1.4, 1.2, −3.9, −20, −34, −67 ppm.

**$L^{tBu,iPr2}Fe(SPh)(MeIm)$.** In a 20 mL scintillation vial, *N*-methylimidazole (20 $\mu$L, 0.251 mmol) was added dropwise via syringe to a red-orange solution of $L^{tBu,iPr2}Fe(SPh)$ (80.8 mg, 0.121 mmol) in $Et_2O$ (10 mL). Upon swirling the solution, an orange solid precipitated immediately. Placing in the freezer (−35 °C) overnight gave a fluffy orange solid (81.7 mg, 90%). This complex can be crystallized from benzene. $^1$H NMR ($C_6D_6$, 500 MHz): $\delta$ 49, 27, 23, 22, 12, 1.2, 2.0, 5.6, 20, 28, 48, 89 ppm. IR (KBr): 3110 (w), 2966 (s), 2866 (m), 1578 (m), 1533 (m), 1489 (s), 1466 (m), 1433 (m), 1379 (s), 1356 (vs), 1315 (s), 1284 (w), 1252 (w), 1217 (m), 1186 (w), 1153 (w), 1099 (m), 1022 (w), 939 (w), 779 (w), 742 (m) cm$^{-1}$. Anal. Calcd for $C_{45}H_{64}N_4SFe$: C, 72.17; H, 8.61; N, 7.46%. Found: C, 72.82; H, 8.71; N, 6.93%.

**UV−vis Equilibrium Experiments.** Three-coordinate iron complexes were dissolved in toluene and filtered through a plug of Celite before adding any reagent(s). Fitting used KaleidaGraph 3.6.2 (Synergy Software). For weak binding, the plot of $[L]_0$ versus $\Delta A_{\lambda max}$ was fit to eq 3 with refinement of the binding constant $K_{eq}$ and a scaling factor. For strong binding, the plot of $[L]_0$ versus $\Delta A_{\lambda max}$ was fit to eq 4 with refinement of $[M]_0$, $K_{eq}$, and a scaling factor. It was necessary to refine $[M]_0$ because the quality of the fit was drastically affected by small variations in

$[M]_0$, which are unavoidable because of small amounts of decomposition. The refined value of $[M]_0$ was always between 0.8 mM and 1.1 mM, consistent with the intended 1.0 mM concentration of iron complex.

**Computations.** The SolidG program[42] was used to calculate cone and solid angles for the neutral ligand of interest. The program utilizes the crystallographic information file (CIF) of a crystal structure to determine spatial orientation of a ligand. The values in Table 5 reflect the average solid and cone angles determined from 10 structures. We used our crystallographic coordinates for DMF and CN$^t$Bu complexes (Figure 4). To supplement these data, we used the Cambridge Structural Database (CSD) to find other iron complexes containing these and other ligands of interest.[1] Priority was given to four-coordinate iron(II) complexes. When necessary, complexes with an increased coordination number and/or strong-field ligands were also used. Because of the scarcity of iron complexes with 2-picoline as a ligand, cobalt and nickel complexes were used to determine the cone and solid angles of this ligand. A full listing of complexes used is in the Supporting Information.

The p$K_a$ of CN$^t$Bu was calculated through means of the acid−base reactions

$$^t\text{BuNCH}^+ + \text{B} \rightarrow {}^t\text{BuNCH} + \text{BH}^+ \quad (6)$$

where B is a reference base whose p$K_a$ is already known experimentally. This approach [43] bypasses the treatment of the solvated proton, whose chemical structure is often unknown and difficult to model theoretically.

The p$K_a$ of $^t$BuNCH$^+$ can be determined by calculating the total free energy change of eq 6:

$$\text{p}K_a(^t\text{BuNCH}^+) = \text{p}K_a(\text{BH}^+) + \frac{\Delta G}{2.303RT} \quad (7)$$

The total free energy change ($\Delta G$) can be evaluated as a combination of gas-phase free energies and solvation free energies:

$$\Delta G = \Delta G_g(^t\text{BuNCH}^+) - \Delta G_g(\text{BH}^+) + \Delta G_{solv}(^t\text{BuNC}) + \Delta G_{solv}(\text{BH}^+) - \Delta G_{solv}(^t\text{BuNCH}^+) - \Delta G_{solv}(\text{B}) \quad (8)$$

where $\Delta G_g(^t\text{BuNCH}^+)$ represents the gas-phase free energy change of the deprotonation reaction, $^t\text{BuNCH}^+ \rightarrow {}^t\text{BuNC} + \text{H}^+$.

The gas-phase geometry optimization and free energy calculation were performed at the B3LYP/6-311++G(d,p) level of theory. The solvation free energies in MeCN were obtained using the Polarizable Continuum Model (PCM) at the B3LYP/6-31+G(d) level. The gas-phase optimized geometries were used for all of the solution-phase calculations.

From the gas-phase free energies and solvation free energies, we can obtain the p$K_a$ of $^t$BuNCH$^+$ using eq 7. In our calculations, we chose several bases as our reference: $PhNH_2$ (experimental p$K_a$ = 10.6); $Et_3N$ (experimental p$K_a$ = 18.8); pyridine (experimental p$K_a$ = 12.5); and, $PhNMe_2$ (experimental p$K_a$ = 11.4).[53] Using these reference bases gave p$K_a$ values for $^t$BuNCH$^+$ of 2.70, 2.82, 3.11, and 2.23, respectively. We take the average value of 2.71 as the p$K_a$ of $^t$BuNCH$^+$ in MeCN.

**Acknowledgment.** The authors thank William Jones and Joseph Dinnocenzo for valuable input and discussions, and thank Eleni Skrombolas for initial experiments. This work was funded by the National Institutes of Health (Grant GM065313 to P.L.H.) and the Department of Education (GAANN fellowship to K.P.C.).

**Supporting Information Available:** Details of NMR spectra, equilibrium measurements, cyclic voltammetry, solid angle calculation (PDF) and crystallography (CIF). This material is available free of charge via the Internet at http://pubs.acs.org.

(53) Kaljurand, I.; Kutt, A.; Soovali, L.; Rodima, T.; Maemets, V.; Leito, I.; Koppel, I. A. *J. Org. Chem.* **2005**, *70*, 1019–1028.